actuators

MDPI

Communication

Extended-State-Observer-Based Super Twisting Control for Pneumatic Muscle Actuators

Yu Cao, Zhongzheng Fu *, Mengshi Zhang and Jian Huang

The Key Laboratory of Image Processing and Intelligent Control, School of Artificial Intelligence and Automation, Huazhong University of Science and Technology, Wuhan 430074, China; cao_yu@mail.hust.edu.cn (Y.C.); dream_poem@hust.edu.cn (M.Z.); huang_jan@mail.hust.edu.cn (J.H.)

* Correspondence: fzzracing@outlook.com; Tel.: +86-27-8754-3130

Abstract: This paper presents a tracking control method for pneumatic muscle actuators (PMAs). Considering that the PMA platform only feedbacks position, and the velocity and disturbances cannot be observed directly, we use the extended-state-observer (ESO) for simultaneously estimating the system states and disturbances by using measurable variables. Integrated with the ESO, a super twisting controller (STC) is design based on estimated states to realize the high-precision tracking. According to the Lyapunov theorem, the stability of the closed-loop system is ensured. Simulation and experimental studies are conducted, and the results show the convergence of the ESO and the effectiveness of the proposed method.

Keywords: extended-state-observer; super twisting control; pneumatic muscle actuator

Citation: Cao, Y.; Fu, Z.; Zhang, M.; Huang, J. Extended-State-Observer-Based Super Twisting Control for Pneumatic Muscle Actuators. *Actuators* **2021**, *10*, 35. https://doi.org/10.3390/act10020035

Academic Editor: Gary M. Bone

Received: 31 December 2020
Accepted: 15 February 2021
Published: 18 February 2021

1. Introduction

In recent years, pneumatic muscle actuators (PMAs), a kind of bio-inspired actuator, have gradually become an important research branch in the robotic field [1–3] because soft actuators improve the system's flexibility and further promote the safety and comfort of human-computer interaction [4,5]. Remarkably, because of the advantages of simple structure, light material, and high power-weight ratio, PMAs are widely used in the robot field, such as robot arms [6], and exoskeletons [7–9] etc. However, the PMA's elastic deformation and friction lead to the features of nonlinearities, uncertainties, time-varying parameters, and hysteresis etc. [10], causing the PMA challenging to be modeled and controlled accurately.

Currently, PMA's control approaches can be mainly divided into two categories: model-based control methods and model-free ones. Model-free control algorithms include the proportional-integral-derivative (PID) control [11–13], neural network control [14,15], fuzzy control [16,17], model-free adaptive control [18], etc. However, PID control has poor tracking performance when it handles the problem with strong nonlinearity. The model-free adaptive control suffers from low tracking accuracy and poor robustness when the adaptive gain is too large or too small. Besides, both neural networks and fuzzy control belong to intelligent control methods whose global approximation capability makes them very suitable for applications in nonlinear uncertain systems [19]. However, they may bring a great computational burden to the system when they handle large scale neurons or complex information. On the other hand, the model-based control algorithms can better handle system uncertainties/disturbances and improve the robustness. One of the most widely used model-based algorithms is the sliding mode control (SMC), which contains a discontinuous function to force the system states always on the sliding surfaces [20,21]. It is remarkable that the sliding surfaces are independent of the plant parameters and disturbances so that the SMC has strong robustness to parameter uncertainties and external disturbances. However, the bandwidths of sensors and actuators are limited in physical applications, resulting in a severe chattering phenomenon. Several methods have

been investigated to deal with this problem. Huang presented a high-order disturbance observer-based SMC to alleviate the chattering phenomenon for underactuated robotic systems [22,23]. Proxy-based robust control assumes a non-zero mass proxy between the controlled object and the desired trajectory, improving tracking safety and eliminating the chattering simultaneously [24,25]. Another branch methods are high-order SMC where super twisting control (STC), a typical second-order SMC, is widely used. Since the discontinuous term in STC proceeds on the second-order time derivative, the STC is capable of effectively reducing the chattering and converge in finite-time [26]. At present, STC has been widely used in the study of various applications, including four-rotor UAV tracking [27], mobile wheel inverted pendulum system [28]. Generally, the controller design requires the PMA's position and speed feedback. Nevertheless, the general PMA system only feedbacks position, and the velocity cannot be observed directly. A standard method is to use the state observer to realize speed observation, and such observers can estimate system states and disturbances simultaneously so that the robustness of the system can be significantly improved. The common observer is called extended-state-observer (ESO), which regards all factors affecting the plant, including the nonlinear dynamics, uncertainties, and the external disturbances as a total disturbance to be observed [29]. Thus, it can estimate the uncertainties along with the states of the system, enabling disturbance rejection or compensation. It is worth noting that although some studies have shown the control of PMA by STC, it is often assumed that all system states, including displacement and velocity, are observable. In fact, the velocity of the PMA cannot be directly observed. Thus, we introduce an ESO to estimate the unobservable variables, including velocity and disturbances. Although the ESO and STC have been widely used, to the best of our knowledge, there were few studies combining these methods for the PMA system, and there is no successful case in this aspect. Also, the related studies were often used to control the electromechanical systems with fast response. However, unlike the motor, the response of the PMA system is rather slow. It is still meaningful to carry out relevant research to verify whether this method can be used to control PMAs.

In this paper, we propose an ESO-based STC for high-precision tracking of PMAs. Based on the dynamical model of the PMA, the ESO enables the system states and disturbances to be estimated by using the measurable variables, and the stability analysis of the ESO indicates that the estimated errors are ultimately uniformly bounded. Due to the unobservable of the PMA's motion speed and disturbances, the ESO is integrated into the STC by defining the sliding manifold with state estimations. Based on the Lyapunov theorem, the stability of the closed-loop system is guaranteed, and the simulation and experimental studies show the effectiveness and superiorities of the proposed ESO-STC. Since the proposed method presents well in the PMA tracking control, it has a good prospect of becoming an excellent pneumatic rehabilitation robot control approach.

The rest of this paper is organized as follows. In Section 2, the three-element-model of the PMA with disturbances is presented. The STC with the ESO is designed in Section 3. Section 4 performs numerical simulation shows the effectiveness of the proposed method, and experiments studies compare the performance of the proposed controller with those of the traditional STC and the PID controller. The final section provides some concluding comments.

2. Problem Formulation

The typical manufacture of the PMA is an elastic rubber tube wrapped in the braided mesh shell. When the inner air pressure of the PMA increases, the rubber tube expands, the diameter largens in the radial direction and the length decreases in the axial direction, simultaneously. In this situation, the braided mesh shell limits the excessive expansion of the rubber tube. While the PMA is deflated, it will return to its original length, due to the elasticity of the rubber tube. Therefore, even if there is no load to pull, the PMA will return to its original length after deflation. This means that without additional load, the internal

air pressure of the PMA determines its displacement. In the case of additional load, the displacement of the PMA is related to the resultant force exerted on the PMA.

The dynamics of a PMA is usually described by using the Three-element-model which is comprised of a spring element, a damping element and a contractile element in parallel [30]. Its dynamics is formulated by:

$$\begin{cases} m\ddot{x} + b(P)\dot{x} + k(P)x = f(P) - mg \\ b(P) = b_0 + b_1 P \\ k(P) = k_0 + k_1 P \\ f(P) = f_0 + f_1 P \end{cases} \tag{1}$$

where x is the PMA displacement. m is the load mass. g is the acceleration of gravity. $b(P)$, $k(P)$ and $f(P)$ are the damping element, the spring element and the contractile force, respectively. b_0, b_1, k_0, k_1, f_0 and f_1 are model parameters. The inner pressure of a PMA P can be dented as the control signal. Remarkably, the damping coefficients vary with inflation and deflation, so the damping element is expressed as:

$$\begin{cases} b(P) = b_{0i} + b_{1i} P \quad (inflation) \\ b(P) = b_{0d} + b_{1d} P \quad (deflation) \end{cases} \tag{2}$$

Whereas the parameters of the Three-element-model are difficult to be identified such that the system uncertainties, including unmodel dynamics, friction and inaccurate parameters, etc., cannot avoid. The dynamics of the PMA can be rewritten with the disturbances denoted as d.

$$\begin{cases} \dot{x}_1 = x_2 \\ \dot{x}_2 = g_0 u + d^* \\ d^* = f(x_1, x_2) + \Delta g \cdot u + d \end{cases} \tag{3}$$

with

$$\begin{cases} f(x_1, x_2) = \frac{1}{m}(f_0 - mg - b_0 x_2 - k_0 x_1) \\ g(x_1, x_2) = g_0 + \Delta g = \frac{1}{m}(f_1 - b_1 x_2 - k_1 x_1) \end{cases}$$

where $f(x_1, x_2)$ and $g(x_1, x_2)$ are nonlinear terms. g_0 is a constant and Δg is the unknown increment. u is the inner pressure. d^* is the augmented disturbances that contain the information of the lumped disturbances d and nonlinear terms.

Assumption 1. *The unknown lumped disturbance d^* is continuous and its derivative satisfies*

$$\left|\dot{d}^*\right| \leq \varepsilon_m \tag{4}$$

where ε_m is an unknown positive constant.

Lemma 1. *[31] Given a differentiable continuous function $\Psi(t)$ satisfying*

$$\sigma_1 \leq |\Psi(t)| \leq \sigma_2 \tag{5}$$

with positive constant σ_1 and σ_2. The derivative $\dot{\Psi}(t)$ is also bounded.

3. Extended-State-Observer-Based Super Twisting Control for PMAs

3.1. Extended-State-Observer

In the PMA plant, the state x_1 is directly measured by a displacement sensor. However, most of the controller needs the all state information, so first we reconstruct the other states of the system by using the ESO in the following form:

$$\dot{\hat{x}}_1 = \hat{x}_2 + \beta_1(x_1 - \hat{x}_1) \tag{6}$$
$$\dot{\hat{x}}_2 = \hat{d}^* + \beta_2(x_1 - \hat{x}_1) + g_0 u \tag{7}$$
$$\dot{\hat{d}}^* = \beta_3(x_1 - \hat{x}_1) \tag{8}$$

where $\hat{x}_1$ and $\hat{x}_2$ are the estimations of x_1 and x_2, respectively. $\hat{d}^*$ is the estimation of d^*. β_1, β_2 and β_3 are selected to ensure the stability of the ESO.

Let $\tilde{x}_1 = x_1 - \hat{x}_1$, $\tilde{x}_2 = x_2 - \hat{x}_2$ and $\tilde{d}^* = d^* - \hat{d}^*$ the state errors. From (3)–(8), the system can be denoted as:

$$\dot{\tilde{x}}_1 = \dot{x}_1 - \dot{\hat{x}}_1 = -\beta_1\tilde{x}_1 + \tilde{x}_2 \tag{9}$$
$$\dot{\tilde{x}}_2 = \dot{x}_2 - \dot{\hat{x}}_2 = -\beta_2\tilde{x}_1 + \tilde{d}^* \tag{10}$$
$$\dot{\tilde{d}}^* = \dot{d}^* - \dot{\hat{d}}^* = -\beta_3\tilde{x}_1 + \dot{d}^* \tag{11}$$

The state error $\tilde{\boldsymbol{X}} = [\tilde{x}_1, \tilde{x}_2, \tilde{d}^*]^T$ is defined to rewrite (9)–(11) as:

$$\dot{\tilde{\boldsymbol{X}}} = \boldsymbol{A}_1\tilde{\boldsymbol{X}} + \boldsymbol{B}_1 \tag{12}$$
$$\boldsymbol{A}_1 = \begin{bmatrix} -\beta_1 & 1 & 0 \\ -\beta_2 & 0 & 1 \\ -\beta_3 & 0 & 0 \end{bmatrix}, \boldsymbol{B}_1 = \begin{bmatrix} 0 \\ 0 \\ \dot{d}^* \end{bmatrix} \tag{13}$$

According to (12) and (13), it is always possible to select β_1, β_2 and β_3 in such a way that the eigenvalues of $\boldsymbol{A}_1$ are in the left hand plane, by which it is possible to find a positive definite matrix $\mathbf{P}_1$ such that

$$\boldsymbol{A}_1^T\boldsymbol{P}_1 + \boldsymbol{P}_1\boldsymbol{A}_1 = -\boldsymbol{Q}_1 \tag{14}$$

for any given positive definite matrix $\boldsymbol{Q}_1$. Defining a Lyapunov candidate

$$V(\tilde{\boldsymbol{X}}) = \tilde{\boldsymbol{X}}^T\boldsymbol{P}_1\tilde{\boldsymbol{X}} \tag{15}$$

and evaluating $\dot{V}(\tilde{\boldsymbol{X}})$ along (15)

$$\begin{aligned} \dot{V}(\tilde{\boldsymbol{X}}) &= \dot{\tilde{\boldsymbol{X}}}^T\boldsymbol{P}_1\tilde{\boldsymbol{X}} + \tilde{\boldsymbol{X}}^T\boldsymbol{P}_1\dot{\tilde{\boldsymbol{X}}} \\ &= (\boldsymbol{A}_1\tilde{\boldsymbol{X}} + \boldsymbol{B}_1)^T\boldsymbol{P}_1\tilde{\boldsymbol{X}} + \tilde{\boldsymbol{X}}^T\boldsymbol{P}_1(\boldsymbol{A}_1\tilde{\boldsymbol{X}} + \boldsymbol{B}_1) \\ &= \tilde{\boldsymbol{X}}^T\boldsymbol{A}_1^T\boldsymbol{P}_1\tilde{\boldsymbol{X}} + \tilde{\boldsymbol{X}}^T\boldsymbol{P}_1\boldsymbol{A}_1\tilde{\boldsymbol{X}} + 2\boldsymbol{B}_1^T\boldsymbol{P}_1\tilde{\boldsymbol{X}} \\ &= -\tilde{\boldsymbol{X}}^T\boldsymbol{Q}_1\tilde{\boldsymbol{X}} + 2\boldsymbol{B}_1^T\boldsymbol{P}_1\tilde{\boldsymbol{X}} \\ &\leq -\lambda_m(\boldsymbol{Q}_1)\left\|\tilde{\boldsymbol{X}}\right\|^2 + 2\varepsilon_m\|\boldsymbol{P}_1\|\left\|\tilde{\boldsymbol{X}}\right\| \\ &= -\left\|\tilde{\boldsymbol{X}}\right\|(\lambda_m(\boldsymbol{Q}_1)\left\|\tilde{\boldsymbol{X}}\right\| - 2\varepsilon_m\|\boldsymbol{P}_1\|) \end{aligned} \tag{16}$$

After a sufficiently long time, the norm of the state error $\tilde{\boldsymbol{X}}$ is bounded by

$$\left\|\tilde{\boldsymbol{X}}\right\| \leq \frac{2\varepsilon_m\|\boldsymbol{P}_1\|}{\lambda_m(\boldsymbol{Q}_1)} \tag{17}$$

where $\lambda_m(\cdot)$ is the smallest eigenvalue of a matrix. Therefore, the estimation error of the disturbance $\tilde{d}^*$ is bounded, and according to Lemma 1, the derivative of $\tilde{d}^*$ is bounded by:

$$\left|\dot{\tilde{d}}^*\right| < L \tag{18}$$

where L is a positive constant.

3.2. Extended-State-Observer-Based Super Twisting Control

The control object of the PMA is to drive the displacement to track the desired trajectory. In this paper, the STC is considered to realize this task. First, the sliding manifolds are defined as:

$$s = c_1 e_1 + \hat{e}_2 = c_1(x_1 - x_{1d}) + (\hat{x}_2 - x_{2d}) \tag{19}$$

where c_1 is a positive constant. x_{1d} is the desired trajectory, and $x_{2d} = \dot{x}_{1d}$. $e_1 = x_1 - x_{1d}$ is the state error and $\hat{e}_2 = \hat{x}_2 - x_{2d}$ is the error of the state estiamtion.

The scale state variables $\boldsymbol{\psi} = [\psi_1, \psi_2]^T$ are defined as

$$\boldsymbol{\psi} = \begin{bmatrix} \psi_1 \\ \psi_2 \end{bmatrix} = \begin{bmatrix} |s|^{\frac{1}{2}}\mathrm{sgn}(s) \\ -\int_0^t k_2 \mathrm{sgn}(s) d\tau + \tilde{d}^* \end{bmatrix} \tag{20}$$

The derivatives of ψ_1 and ψ_2 are given by:

$$\begin{aligned} \dot{\psi}_1 &= \frac{d|s|^{\frac{1}{2}}\mathrm{sgn}(s)}{dt} = \frac{d|s|^{\frac{1}{2}}}{ds}\frac{ds}{dt}\mathrm{sgn}(s) \\ &= \frac{d|s|^{\frac{1}{2}}}{d|s|}\frac{d|s|}{ds}\frac{ds}{dt}\mathrm{sgn}(s) \\ &= \frac{d|s|^{\frac{1}{2}}}{d|s|}\frac{d\sqrt{s^2}}{ds^2}\frac{ds^2}{ds}\frac{ds}{dt}\mathrm{sgn}(s) \\ &= (\frac{1}{2}|s|^{-\frac{1}{2}})(\frac{1}{2}|s|^{-1})(2s)\dot{s}\mathrm{sgn}(s) \\ &= \frac{1}{2}|s|^{-\frac{1}{2}}\dot{s} = \frac{1}{2|\psi_1|}\dot{s} \end{aligned} \tag{21}$$

$$\begin{aligned} \dot{\psi}_2 &= -k_2\mathrm{sgn}(s) + \dot{\tilde{d}}^* \\ &= |s|^{-\frac{1}{2}}(-k_2|s|^{\frac{1}{2}}\mathrm{sgn}(s) + \dot{\tilde{d}}^*\mathrm{sgn}(s)|s|^{\frac{1}{2}}\mathrm{sgn}(s)) \\ &= \frac{1}{|\psi_1|}(-k_2\psi_1 + \dot{\tilde{d}}^*\mathrm{sgn}(s)\psi_1) \end{aligned} \tag{22}$$

From (3) and (20)–(22), the controller is given by:

$$u = \frac{1}{g_0}(\dot{x}_{2d} - c_1\dot{e}_1 - \beta_2(x_1 - \hat{x}_1) - k_1|s|^{\frac{1}{2}}\mathrm{sgn}(s) - \int_0^t k_2\mathrm{sgn}(s)d\tau - \hat{d}^*) \tag{23}$$

Then, the derivatives of the scale state variables can be rewritten as:

$$\begin{aligned} \dot{\boldsymbol{\psi}} &= \begin{bmatrix} \dot{\psi}_1 \\ \dot{\psi}_2 \end{bmatrix} = \begin{bmatrix} \frac{1}{2|\psi_1|}(-k_1\psi_1 + \psi_2) \\ \frac{1}{|\psi_1|}(-k_2\psi_1 + \dot{\tilde{d}}^*\mathrm{sgn}(s)\psi_1) \end{bmatrix} \\ &= \frac{1}{|\psi_1|}\begin{bmatrix} -\frac{1}{2}k_1 & \frac{1}{2} \\ -k_2 + \dot{\tilde{d}}^*\mathrm{sgn}(s) & 0 \end{bmatrix}\begin{bmatrix} \psi_1 \\ \psi_2 \end{bmatrix} \\ &= \frac{1}{|\psi_1|}\boldsymbol{A}_2\boldsymbol{\psi} \end{aligned} \tag{24}$$

with

$$\boldsymbol{A}_2 = \begin{bmatrix} -\frac{1}{2}k_1 & \frac{1}{2} \\ -k_2 + \dot{\tilde{d}}^*\mathrm{sgn}(s) & 0 \end{bmatrix}$$

Theorem 1. *Using the control (23) for the PMA system (3), the closed-loop system is asymptotically stable.*

Proof. The Lyapunov candidate is defined:

$$V = \boldsymbol{\psi}^T \boldsymbol{P} \boldsymbol{\psi} \tag{25}$$

with

$$\boldsymbol{P} = \begin{bmatrix} p_1 & p_2 \\ p_3 & p_4 \end{bmatrix}$$

where $\boldsymbol{P}$ is a positive matrix.

Remark 1. *Due to the term $\psi_1 = |s|^{1/2} sgn(s)$, the Lyapunov function V is not continuously differentiable on the set $D = \{(\psi_1, \psi_2) \in \mathbb{R}^2 | \psi_1 = 0\}$. Actually, this problem has been addressed in [26]. It proved that the Lyapunov function V is an absolutely continuous function of time on the set $D = \{(\psi_1, \psi_2) \in \mathbb{R}^2 | \psi_1 = 0\}$, and V converges to zero in a finite time if and only if $\dot{V}$ is negative definite almost everywhere [32]. This indicates that V can still be used as a Lyapunov function that ensures the stability of the closed-loop system.*

Evaluating the derivative of (25), it is given by

$$\begin{aligned} \dot{V} &= \dot{\boldsymbol{\psi}}^T \boldsymbol{P} \boldsymbol{\psi} + \boldsymbol{\psi}^T \boldsymbol{P} \dot{\boldsymbol{\psi}} \\ &= (\frac{1}{|\psi_1|} \boldsymbol{A}_2 \boldsymbol{\psi})^T \boldsymbol{P} \boldsymbol{\psi} + \boldsymbol{\psi}^T \boldsymbol{P} (\frac{1}{|\psi_1|} \boldsymbol{A}_2 \boldsymbol{\psi}) \\ &= \frac{1}{|\psi_1|} \boldsymbol{\psi}^T (\boldsymbol{A}_2^T \boldsymbol{P} + \boldsymbol{P} \boldsymbol{A}_2) \boldsymbol{\psi} \end{aligned} \tag{26}$$

Let

$$\mathbf{Q}_2 = -(\mathbf{A}_2^T \mathbf{P} + \mathbf{P} \mathbf{A}_2) \tag{27}$$

When $\mathbf{Q}_2$ is positive definite, $\dot{V} < 0$ is satisfied.

To simplify the expression, $\mathbf{P}$ is assumed to be symmetric and the first element of $\mathbf{P}$ equals 1, $p_2 = p_3$ and $p_1 = 1$. Please note that $\mathbf{Q}_2$ is:

$$\begin{aligned} \mathbf{Q}_2 &= -\begin{bmatrix} -\frac{1}{2}k_1 & -k_2 + \dot{\hat{d}}^* \mathrm{sgn}(s) \\ \frac{1}{2} & 0 \end{bmatrix} \begin{bmatrix} p_1 & p_2 \\ p_3 & p_4 \end{bmatrix} + \begin{bmatrix} p_1 & p_2 \\ p_3 & p_4 \end{bmatrix} \begin{bmatrix} -\frac{1}{2}k_1 & \frac{1}{2} \\ -k_2 + \dot{\hat{d}}^* \mathrm{sgn}(s) & 0 \end{bmatrix} \\ &= -\begin{bmatrix} -k_1 + 2(-k_2 + \dot{\hat{d}}^* \mathrm{sgn}(s)) p_2 & \frac{1}{2} - \frac{1}{2}k_1 p_2 + (-k_2 + \dot{\hat{d}}^* \mathrm{sgn}(s)) p_4 \\ \frac{1}{2} - \frac{1}{2}k_1 p_2 + (-k_2 + \dot{\hat{d}}^* \mathrm{sgn}(s)) p_4 & p_2 \end{bmatrix} \end{aligned} \tag{28}$$

It is remarkable that $\mathbf{P}$ and $\mathbf{Q}_2$ should be positive definite, thus the following inequalities should hold:

$$\begin{cases} p_4 > p_2^2 \\ -k_1 p_2 + 2(-k_2 + \dot{\hat{d}}^* \mathrm{sgn}(s)) p_2^2 - (\frac{1}{2} - \frac{1}{2}k_1 p_2 + (-k_2 + \dot{\hat{d}}^* \mathrm{sgn}(s)) p_4)^2 > 0 \end{cases} \tag{29}$$

We define auxiliary variables $\chi, \alpha, \beta, \gamma$ to satisfy the following equations:

$$k_1 = \chi \sqrt{\frac{2\gamma}{(1-\beta)\alpha}} \sqrt{L}, k_2 = \frac{(\beta+1)}{(1-\beta)} L \tag{30}$$

$$p_1 = 1, p_4 = \frac{(1-\beta)\alpha}{2L}, p_2 = p_3 = -\sqrt{\frac{(1-\beta)\alpha}{2\gamma L}} = -\sqrt{\frac{p_4}{\gamma}} \tag{31}$$

From (18), the following inequality holds.

$$k_2 - L \leq k_2 - \dot{\hat{d}}^* sgn(s) \leq k_2 + L \tag{32}$$

Bringing (30)–(32) into (29), (29) will hold when the auxiliary variables satisfy

$$\begin{cases} \gamma > 1, \chi > 0, 0 < \beta < 1, \alpha > 0 \\ \chi - \frac{2}{\gamma}\alpha > \alpha^2 - \beta(1+\chi)\alpha + \frac{1}{4}(1+\chi)^2 \end{cases} \tag{33}$$

Hence, it is easy to find a set of auxiliary variables to ensure that (29) holds. Consequently, $\dot{V} < 0$.

This completes the proof. □

4. Simulation Studies

In this section, the proposed control method drives the PMA to track the desired trajectory. All the simulations were programmed with MATLAB, version 2013b, and were run on a PC with a clock speed of 3.6 GHz and 8-GB RAM in a Microsoft Windows 10 environment.

The desired trajectory is set as a sinusoidal trajectory, as shown:

$$x_{1d} = A\sin(2\pi w t) + B \tag{34}$$

where $w = 0.25$, $A = 0.015$ m and $B = 0.015$ m are the parameters set accordingly. The control parameters of the ESO-STC are selected as: $\beta_1 = 113.4, \beta_2 = 1.4 \times 10^5, \beta_3 = 1.0 \times 10^6, c_1 = 173.9, k_1 = 7.97, k_2 = 193.6, g_0 = 100.4$.

The performance of the proposed method depends on the ESO, since the controller contains the information of the estimated states $\hat{x}_1$, $\hat{x}_2$ and $\hat{d}^*$. In Figure 1, the estimated state $\hat{x}_1$ tracks the PMA trajectory x_1, which indicates the effectiveness of the ESO. It is remarkable that the tracking error is $\tilde{\mathbf{X}}$ ultimately uniformly bounded, referring to (17), such that the tracking error between x_1 and $\hat{x}_1$ is determined by the ESO's parameters β_1, β_2 and β_3. These parameters should be carefully selected to ensure the smallest eigenvalue of $\boldsymbol{Q}_1$ sufficiently large, then the tracking error $\tilde{\mathbf{X}}$ is small enough to guarantee the high-accuracy convergence of the ESO. The tracking results of the proposed method are shown in Figure 2. The results show that the proposed method can make the PMA track the desired trajectory with relatively high accuracy. Because the STC is a second-order sliding mode control strategy, the controller will not produce serious chattering. This is especially suitable for such slow response systems.

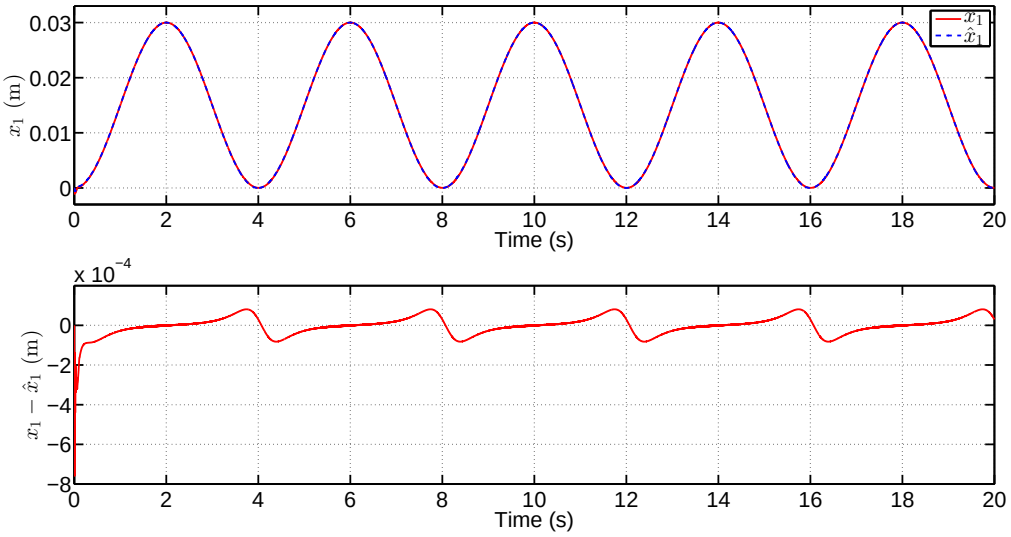

Figure 1. The performance of the ESO.

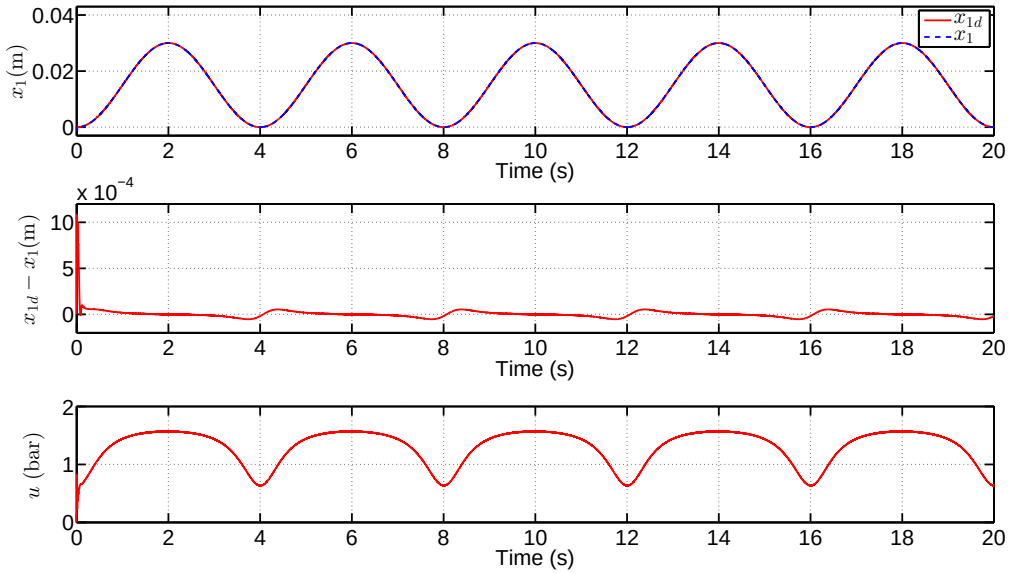

Figure 2. The tracking performance of the proposed method.

In conclusion, the proposed method effectively estimates the system states and drives the PMA to track the desired trajectory.

5. Experimental Studies

The experimental platform is comprised of a PMA, a PMA displacement sensor, an air pressure sensor, an electromagnetic valve, an air compressor, and an acquisition card, as shown in Figure 3. Also, a component called xPC target from Mathworks Inc. is used to establish the software environment in which a host computer and a target computer are required. The MATLAB/SIMULINK and C language compiler are installed in the host computer to generate executable codes, while the target computer directly invokes the hardware resource to run applications in real-time.

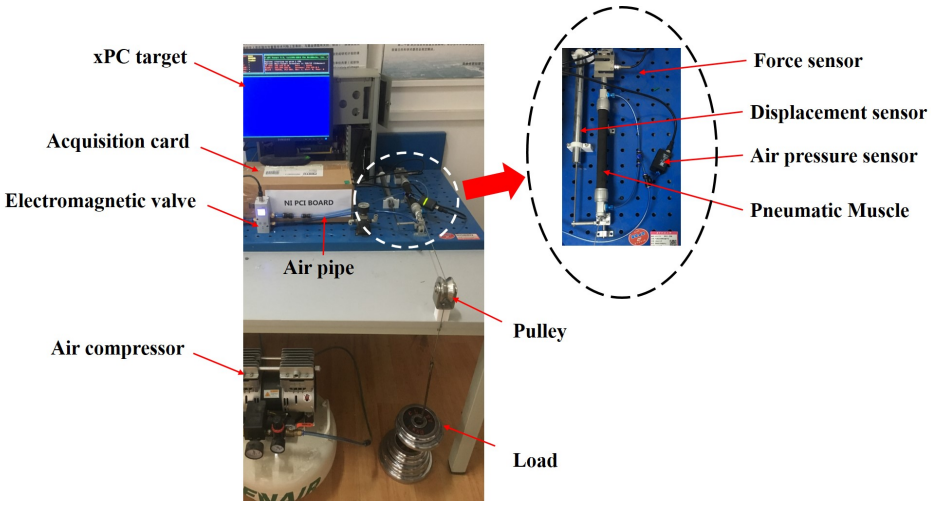

Figure 3. The PMA platform.

In the physical system, the board (NI-PCI 6052E) collects the sensory data and transmits the control signal to the electromagnetic proportional valve. The air compressor (Denair, DW35) provides compressed air and is connected to the PMA through the electromagnetic proportional valve. Consequently, the displacement of the PMA can be controlled by the displacement signals. The PMA is Festo DMSP-20-200N-RM-RM fluidic muscle with an internal diameter of 20 mm, nominal length of 200 mm, and an operating pressure range from 0 to 6 bar. The Festo VPPM-6L-L-1-G18-0L10H-V1P proportional valve is

used to regulate the pressure inside the PMA. The displacement sensor is GA-75 whose measurement range is 0–150 mm.

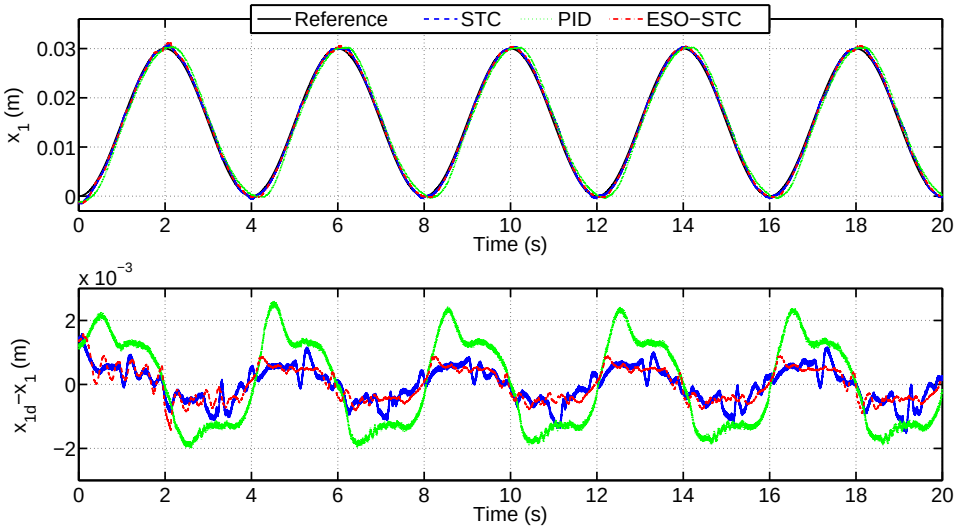

Figure 4. The comparisons of different control methods.

The desired trajectory is the same as the simulation, as shown:

$$x_{1d} = A\sin(2\pi wt) + B \tag{35}$$

where $w = 0.25$, $A = 0.015$ m and $B = 0.015$ m. The integral of absolute error ($Error^a$) and the maximum absolute error ($Error^b$) can measure the tracking performance from two different perspectives:

$$Error^a = \frac{1}{n}\sum_{t=1}^{n}|x_{1d}(t) - x_1(t)| \tag{36}$$

$$Error^b = \max(\sum_{t=1}^{n}|x_{1d}(t) - x_1(t)|_{t=1}^{n}) \tag{37}$$

where n is the total sample of the experiment.

In the physical experimental studies, a PID controller and a STC controller are implemented to compare with the proposed ESO-STC under the same experimental conditions. We tried our best to tune the control parameters of all the strategies to demonstrate the superiorities of the proposed method.

The experimental results are shown in Figure 4 and Table 1. It is shown that all the control strategies can drive the PMA to track the desired trajectory. The PID controller behaves the worst performance because this approach is seriously dependent on the proper control parameters. However, we can just tune the parameters by the trial-and-error method. Therefore, despite our best efforts, its control effect is still poor. On the other hand, it is remarkable that the STC is the fundamental of the ESO-STC in which the ESO is used to estimate $x_2 = \dot{x}_1$, since x_2 cannot be directly measured. When the error between $\dot{x}_1$ and $\hat{x}_2$ is small enough, the STC and the ESO-STC have similar performance. This is because there is no load imposed on the PMA in this experiment. Moreover, the ESO-STC estimates the lumped disturbances of the PMA plant, so that it has better robustness than that of the STC.

To verify the robustness of the proposed method, we conducted an experiment where loads of different masses are suspended at one end of the PMA, $m = \{0\text{ kg}, 1.5\text{ kg}, 2.5\text{ kg}\}$. The result shows that with the increase of the load, the maximum tracking error of the PMA increases gradually, and the controller can deal with the disturbances in a certain range, as shown in Figure 5. When the load is overlarge, the tracking performance of the

system decreases rapidly. The main reason is that when the disturbances caused by load exceeds the limit, the system stability conditions may be violated and the system becomes unstable. In this case, the parameters of the control method need to be re-tuned.

Table 1. Tracking performance of different control strategies.

	$Error^a$	$Error^b$
ESO-STC	4.63×10^{-4} (m)	1.6×10^{-3} (m)
STC	4.63×10^{-4} (m)	1.6×10^{-3} (m)
PID	1.3×10^{-3} (m)	2.6×10^{-3} (m)

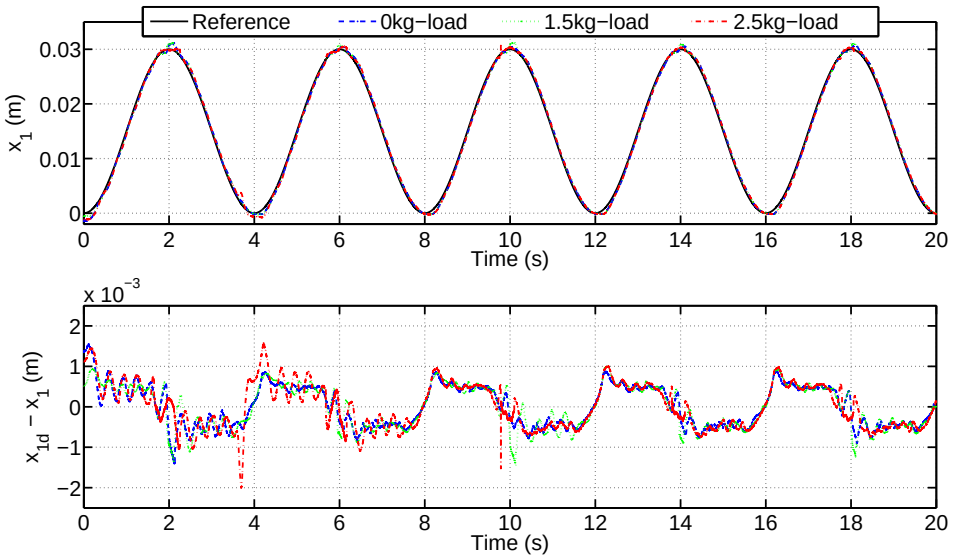

Figure 5. Different loads are suspended to verify the robustness of the ESO-STC.

6. Conclusions

Due to the advantages of simple structure, light material, and high power-weight ratio, the PMA has become a widely used actuator in the robotic field. However, its intrinsically soft characteristics make its precise control still a challenge. Traditional methods often assume that all system states, including displacement and velocity, are observable. However, the velocity of the PMA cannot be directly observed, and the system uncertainties need to be handled in physical applications. In this paper, the ESO is introduced to simultaneously estimate the unobservable states and disturbances, and integrated with the STC to realize disturbance rejection or compensation. The stability of the closed-loop system is ensured, and simulations and experiments are conducted. The results show that the proposed method is a chattering-free algorithm, and it can realize the high-precision tracking of the PMA and improve the system robustness.

Author Contributions: Conceptualization, Y.C., Z.F., M.Z. and J.H.; methodology, M.Z.; validation, Y.C.; software, Y.C. All authors have read and agreed to the published version of the manuscript.

Funding: This work was supported in part by the Joint fund of Science and Technology Department of Liaoning Province and State Key Laboratory of Robotics, China, in part by the Innovation Fund of WNLO, and in part by the Fundamental Research Funds for the Central Universities under Grant HUST: 2019kfyXKJC019, 2019kfyRCPY014.

Institutional Review Board Statement: Not applicable.

Informed Consent Statement: Not applicable.

Data Availability Statement: The data presented in this study are available on request from the corresponding author.

Acknowledgments: The authors would like to thank the anonymous reviewers who greatly help to improve this paper.

Conflicts of Interest: The authors declare no conflict of interest.

Abbreviations

The following abbreviations are used in this manuscript:

PMA	Pneumatic Muscle Actuator
SMC	Sliding Mode Control
ESO	Extended-state-observer
STC	Super Twisting Control
PID	Proportional-Integral-Derivative
ESO-STC	Extended-state-observer-based Super Twisting Control

References

1. Zhang, J.; Sheng, J.; O'Neill, C.T.; Walsh, C.J.; Wood, R.J.; Ryu, J.; Desai, J.P.; Yip, M.C. Robotic artificial muscles: Current progress and future perspectives. *IEEE Trans. Robot.* **2019**, *35*, 761–781. [CrossRef]
2. Laschi, C.; Mazzolai, B.; Cianchetti, M. Soft robotics: Technologies and systems pushing the boundaries of robot abilities. *Sci. Robot.* **2016**, *1*, eaah3690. [CrossRef]
3. Takosoglu, J.E.; Laski, P.A.; Blasiak, S.; Bracha, G.; Pietrala, D. Determining the Static Characteristics of Pneumatic Muscles. *Meas. Control* **2016**, *49*, 62–71. [CrossRef]
4. Rus, D.; Tolley, M.T. Design, fabrication and control of soft robots. *Nature* **2015**, *521*, 467–475. [CrossRef]
5. Cao, Y.; Huang, J.; Ru, H.; Chen, W.; Xiong, C.-H. A Visual Servo Based Predictive Control with Echo State Gaussian Process for Soft Bending Actuator. *IEEE/ASME Trans. Mechatron.* **2020**. [CrossRef]
6. Deimel, R.; Brock, O. A novel type of compliant and underactuated robotic hand for dexterous grasping. *Int. J. Robot. Res.* **2016**, *35*, 161–185. [CrossRef]
7. Cao, Y.; Huang, J. Neural-network-based nonlinear model predictive tracking control of a pneumatic muscle actuator-driven exoskeleton. *IEEE/CAA J. Autom. Sin.* **2020**, *7*, 1478–1488. [CrossRef]
8. Bharadwaj, K.; Sugar, T.G. Kinematics of a robotic gait trainer for stroke rehabilitation. In Proceedings of the 2006 IEEE International Conference on Robotics and Automation, Orlando, FL, USA, 15–19 May 2006; pp. 3492–3497.
9. Cao, Y.; Huang, J.; Xiong, C. Single-layer Learning Based Predictive Control with Echo State Network for Pneumatic Muscle Actuators-driven Exoskeleton. *IEEE Trans. Cognit. Dev. Syst.* **2020**. [CrossRef]
10. Caldwell, D.G.; Medrano-Cerda, G.A.; Goodwin, M. Control of pneumatic muscle actuators. *IEEE Control Syst.* **1995**, *15*, 40–48.
11. Andrikopoulos, G.; Nikolakopoulos, G.; Manesis, S. Advanced Nonlinear PID-Based Antagonistic Control for Pneumatic Muscle Actuators. *IEEE Trans. Ind. Electron.* **2014**, *61*, 6926–6937. [CrossRef]
12. Zhang, D.; Zhao, X.; Han, J. Active Model-Based Control for Pneumatic Artificial Muscle. *IEEE Trans. Ind. Electron.* **2017**, *64*, 1686–1695. [CrossRef]
13. Takosoglu, J. Angular position control system of pneumatic artificial muscles. *Open Eng.* **2020**, *10*, 681–687. [CrossRef]
14. Huang, J.; Cao, Y.; Xiong, C.-H.; Zhang, H.-T. An echo state Gaussian process-based nonlinear model predictive control for pneumatic muscle actuators. *IEEE Trans. Autom. Sci. Eng.* **2018**, *16*, 1071–1084. [CrossRef]
15. Zhong, J.; Zhou, X.; Luo, M. A New Approach to Modeling and Controlling a Pneumatic Muscle Actuator-Driven Setup Using Back Propagation Neural Networks. *Complexity* **2018**, *2018*, 1–9. [CrossRef]
16. Chen, C.; Huang, J.; Wu, D. Nonlinear Disturbance Observer Based TS Fuzzy Logic Control of Pneumatic Artificial Muscles. In Proceedings of the 2019 IEEE 4th International Conference on Advanced Robotics and Mechatronics (ICARM), Osaka, Japan, 3–5 July 2019; pp. 12–17.
17. Nuchkrua, T.; Leephakpreeda, T.; Chen, S.L. Experimental validation for fuzzy control of servo pneumatic artificial muscle driven by metal hydride. *Int. J. Fuzzy Syst.* **2016**, *18*, 956–970. [CrossRef]
18. Sun, N.; Liang, D.; Wu, Y.; Chen, Y.; Qin, Y.; Fang, Y. Adaptive control for pneumatic artificial muscle systems with parametric uncertainties and unidirectional input constraints. *IEEE Trans. Ind. Inform.* **2019**, *16*, 969–979. [CrossRef]
19. Huang, J; Ri, M; Wu, D. Interval Type-2 Fuzzy Logic Modeling and Control of a Mobile Two-Wheeled Inverted Pendulum. *IEEE Trans. Fuzzy Syst.* **2018**, *26*, 2030–2038. [CrossRef]
20. Xing, K.; Huang, J.; Wang, Y.; Wu, J.; Xu, Q.; He, J. Tracking control of pneumatic artificial muscle actuators based on sliding mode and non-linear disturbance observer. *IET Control Theory Appl.* **2010**, *4*, 2058–2070. [CrossRef]
21. Aschemann, H.; Schindele, D. Sliding-mode control of a high-speed linear axis driven by pneumatic muscle actuators. *IEEE Trans. Ind. Electron.* **2008**, *55*, 3855–3864. [CrossRef]
22. Huang, J.; Zhang, M.; Ri, S.; Xiong, C.; Li, Z.; Kang, Y. High-Order Disturbance-Observer-Based Sliding Mode Control for Mobile Wheeled Inverted Pendulum Systems. *IEEE Trans. Ind. Electron.* **2020**, *67*, 2030–2041. [CrossRef]

23. Huang, J.; Ri, S.; Fukuda, T.; Wang, Y. A Disturbance Observer Based Sliding Mode Control for a Class of Underactuated Robotic System With Mismatched Uncertainties. *IEEE Trans. Autom. Control* **2019**, *64*, 2480–2487. [CrossRef]
24. Cao, Y.; Huang, J.; Xiong, C.-H.; Wu, D.; Zhang, M.; Li, Z.; Hasegawa, Y. Adaptive Proxy-Based Robust Control Integrated With Nonlinear Disturbance Observer for Pneumatic Muscle Actuators. *IEEE/ASME Trans. Mechatron.* **2020**, *25*, 1756–1764. [CrossRef]
25. Huang, J.; Cao, Y.; Wang, Y.-W. Adaptive proxy-based sliding mode control for a class of second-order nonlinear systems and its application to pneumatic muscle actuators. *ISA Trans.* **2020**. [CrossRef] [PubMed]
26. Moreno, J.A.; Osorio, M. Strict Lyapunov Functions for the Super-Twisting Algorithm. *IEEE Trans. Autom. Control* **2012**, *57*, 1035–1040. [CrossRef]
27. Derafa, L.; Benallegue, A.; Fridman, L. Super twisting control algorithm for the attitude tracking of a four rotors UAV. *J. Frankl. Inst.* **2012**, *349*, 685–699. [CrossRef]
28. Zhang, M.; Huang, J.; Cao, Y. Adaptive Super-Twisting Control for Mobile Wheeled Inverted Pendulum Systems. *Appl. Sci.* **2019**, *9*, 2508. [CrossRef]
29. Talole, S.E.; Kolhe, J.P.; Phadke, S.B. Extended-State-Observer-Based Control of Flexible-Joint System With Experimental Validation. *IEEE Trans. Ind. Electron.* **2010**, *57*, 1411–1419. [CrossRef]
30. Reynolds, D.B.; Repperger, D.W.; Phillips, C.A.; Bandry, G. Modeling the dynamic characteristics of pneumatic muscle. *Ann. Biomed. Eng.* **2003**, *31*, 310–317. [CrossRef]
31. Zhang, L.; Li, Z.; Yang, C. Adaptive Neural Network Based Variable Stiffness Control of Uncertain Robotic Systems Using Disturbance Observer. *IEEE Trans. Ind. Electron.* **2017**, *64*, 2236–2245. [CrossRef]
32. Baccioti, A.; Rosier, L. *Liapunov Functions and Stability in Control Theory*, 2nd ed.; Springer: New York, NY, USA, 2005.